THE JOURNAL OF PHYSICAL CHEMISTRY C

pubs.acs.org/JPCC Article

Transition from H-Aggregate Nanotubes to J-Aggregate Nanoribbons

Samuel Rhodes,[#] Wenlang Liang,[#] Xiaochen Wang, Nitin Ramesh Reddy, and Jiyu Fang*

Cite This: J. Phys. Chem. C 2020, 124, 11722–11729 Read Online

ACCESS | Metrics & More | Article Recommendations | Supporting Information

ABSTRACT: J- and H-aggregates of π-conjugated dyes are particularly interesting because of their unique optical and excitonic properties. However, control of the size and morphology of J- and H-aggregates remains a challenge. Here, we report the coassembly of lithocholic acid (LCA) and 3,3′-diethylthiacarbocyanine iodide ($DiSC_2(3)$) into H-aggregate nanotubes through helical H-aggregate nanoribbons as a precursor in 30% ammonia solution. As the ammonia evaporates, H-aggregate nanotubes transition into flat J-aggregate nanoribbons. The electronic properties of H-aggregate nanotubes and J-aggregate nanoribbons are studied by integrating them with interdigitated gold electrodes. We find that H-aggregate nanotubes form a Schottky junction and J-aggregate nanoribbons form Ohmic contact. In the temperature range from 18 to 28 °C, the resistance of the H-aggregate nanotubes is nearly constant, whereas the resistance of the J-aggregate nanoribbons significantly increases with the increase of temperature. Our findings provide a new strategy for controlling the formation of H-aggregate nanotubes and J-aggregate nanoribbons, which can serve as smart building blocks in electronic and optoelectronic devices.

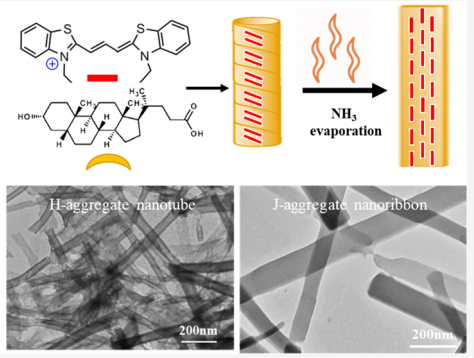

INTRODUCTION

One-dimensional (1D) supramolecular structures ranging from nanofibers to nanoribbons and nanotubes made of π-conjugated molecules are promising building blocks in the fabrication of electronic and optoelectronic devices.[1−5] Among various one-dimensional (1D) supramolecular structures, J- and H-aggregates of π-conjugated dyes are particularly interesting because of their unique optical and excitonic properties.[6] For example, H-aggregates, which are composed of dye molecules in a face-to-face stacking, give rise to a blue-shifted absorption band compared with a monomer band and a strong emission quenching. In contrast, J-aggregates, which are made by an edge-to-edge stacking of dye molecules, show a red-shifted absorption band with respect to a monomer band and a strong fluorescence emission. In past decades, there was great interest in controlling the size and morphology of J- and H-aggregates. Particularly, the self-assembly of amphiphilic dyes was widely used to form J-aggregate nanotubes.[7−15] The coassembly of dyes and surfactants provides a promising approach for forming J-aggregate nanotubes without requiring time-consuming processes for the synthesis of amphiphilic dyes.[16−21] J-aggregate nanotubes have shown great promise as artificial light-harvesting antennas for energy transfer[9,20] and highly efficient photoinduced electron-transfer probes for biosensor applications.[21]

Lithocholic acid (LCA) is a biological surfactant with a chiral steroid skeleton and a carboxyl group linked to the steroid skeleton through a short alkyl chain. It was shown that LCA in alkaline solution could self-assemble into nanotubes through electrostatic interaction, hydrophobic force, and hydrogen bonding. The diameter and shape of LCA nanotubes depend on the condition under which the self-assembly of LCA occurred.[22−28] Here, we report the formation of H-aggregate nanotubes by the coassembly of LCA and 3,3′-diethylthiacarbocyanine iodide ($DiSC_2(3)$) in 30% ammonia solution. The H-aggregate nanotubes transition into flat J-aggregate nanoribbons as the ammonia evaporates. The H- to J-aggregate transition is reversible. After being resuspended in 30% ammonia solution, flat J-aggregate nanoribbons transition back into H-aggregate nanotubes. The structure and optical properties of H-aggregate nanotubes and J-aggregate nanoribbons are characterized to help understand the H- to J-aggregate transition mechanism. The electronic properties of H-aggregate nanotubes and J-aggregate nanoribbons are measured by integrating them on interdigitated gold electrodes.

EXPERIMENTAL SECTION

Sample Preparation. LCA was mixed with $DiSC_2(3)$ at a molar ratio of 5:1 and 1:1 in 30% ammonia solution, for which

Received: April 1, 2020
Revised: April 30, 2020
Published: May 1, 2020

https://dx.doi.org/10.1021/acs.jpcc.0c02908
J. Phys. Chem. C 2020, 124, 11722−11729

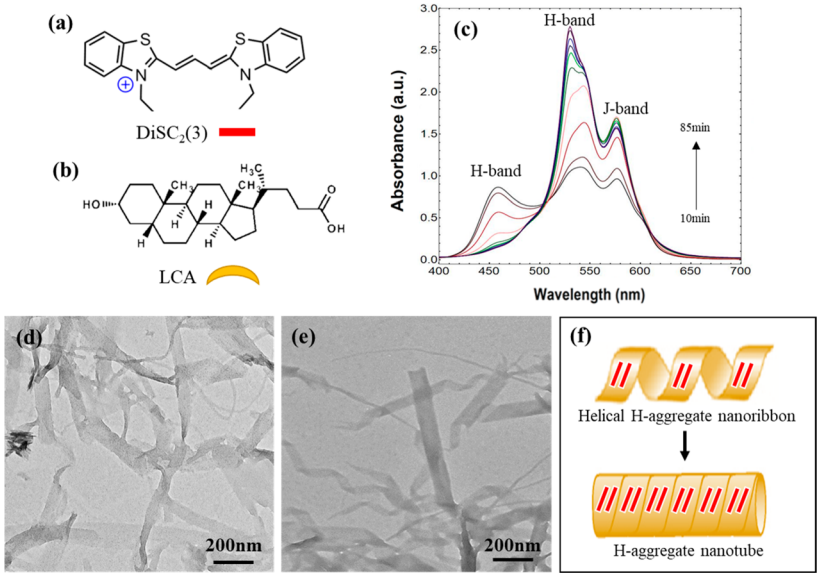

Figure 1. Chemical structures of $DiSC_2(3)$ (a) and LCA (b). (c) Time-dependent adsorption spectra of LCA/$DiSC_2(3)$ solution with a mixed molar ratio of 5:1 in a sealed glass bottle at room temperature. TEM images of twisted H-aggregate nanoribbons, which formed 10 min after the mixed solution was made (d), and helical H-aggregate nanoribbons and nanotubes, which formed 90 min after the mixed solution was made (e). (f) Schematic representation of helical H-aggregate nanoribbons and H-aggregate nanotubes.

the concentration of LCA was always kept at 1 mM. The mixed solution was sonicated at ∼50 °C in an ultrasonic bath (Branson 1510, Branson Ultrasonics Co.) for 5 min and then cooled down to room temperature. After being aged in a sealed or open glass bottle in the dark for a period of time, the mixed solution was characterized.

Spectrum Measurements. J- and H-aggregate solution was added to a quartz cuvette. The absorption and circular dichroism spectra were taken with a Cary 60 spectrophotometer and a JASCO J-815 spectropolarimeter, respectively. The fluorescence spectra were taken using a Jasco FP-6500 spectrofluorometer. Fourier transform-infrared (FT-IR) spectra were acquired with a PerkinElmer (100) spectrometer operating at 4 cm^{-1} resolution.

Microscopy Observations. Transmission electron microscopy (TEM) measurements were performed on a JEOL TEM-1011 operated at 100 kV. Scanning electron microscopy (SEM) images were taken with a Zeiss Ultra-55 FEG SEM operated at 20 kV. For these electron microscopy measurements, 5 μL of J- and H-aggregate solution was dried on a holey Formvar film at room temperature for 24 h. Height and amplitude atomic force microscopy (AFM) images were taken with a Dimension 3100 from Veeco Instruments; a silicon nitride cantilever (Nanosensors) with a spring constant of 30 N/m was used. Confocal fluorescence images were acquired with a Zeiss Axioscope-2 MOT microscope. For polarizing optical microscopy (POM) observation, a drop of aggregate solution was placed on a glass substrate, followed by placing a cover glass slide on the top of the drop. Polarized optical microscopy (POM) images were captured with a digital camera (C2020 Zoom, Olympus) mounted on an optical microscope (Olympus BX),

Cyclic Voltammetry (CV) Measurements. One hundred microliters of J- and H-aggregate solution was dried on an indium tin oxide (ITO) working electrode at room temperature. CV measurements were performed in an aqueous solution containing 1 M KCl with a CS 350 Electrochemical workstation, for which a platinum wire acted as the counter electrode and Ag/AgCl served as a reference electrode. The scan range was from −0.4 to 0.8 V at the speed of 0.01 V/s.

Electron-Transport Measurements. Five microliters of J- and H-aggregate solution was dropped onto the interdigitated Au electrodes with a 20 μm gap and then dried at room temperature. Current−voltage (I−V) curves were measured with a Keithley 2400 sourcemeter in the temperature range from 18 to 28 °C, which was controlled by an Instec thermal stage.

RESULTS AND DISCUSSION

The chemical structures of $DiSC_2(3)$ and LCA are shown in Figure 1a and Figure 1b, respectively. LCA is a secondary bile acid with a critical micelle concentration of ∼1.0 mM.[29] $DiSC_2(3)$ monomers in methanol showed an absorption band at 556 nm (Figure S1, Supporting Information), which agreed with the result reported in the literature.[30] In a previous publication, we showed that the coassembly of LCA and $DiSC_2(3)$ in 1% ammonia solution could lead to the formation of spherulitic J-aggregates with the J-band at 590 nm.[31] The solubility of $DiSC_2(3)$ was low in 1% ammonia solution. The insoluble $DiSC_2(3)$ served as a nucleation site for the growth of J-aggregate nanofibers from the coassembly of LCA and soluble $DiSC_2(3)$, ultimately forming J-aggregate spherulites. The solubility of $DiSC_2(3)$ in ammonia solution increased with the increase of ammonia concentrations. In 30% ammonia solution, $DiSC_2(3)$ self-assembled into spherical H-aggregates with two H-bands at 360 and 425 nm, together with a monomer band at 556 nm (Figure S2a). The appearance of two H-bands is likely due to Davydov's splitting of the excited-state level of spherical H-aggregates. The diameter of spherical H-aggregates was in the range from 30 to 70 nm (Figure S2b).

Figure 1c shows the time-dependent absorption spectra of mixed LCA/$DiSC_2(3)$ solution with the mixed molar ratio of 5:1. In the early stage (10 min after the mixed solution was made), we observed two H-bands at 457 and 540 nm, together with a J-band at 580 nm. The H-band at 457 nm decreased over time and completely disappeared after 85 min. In the

https://dx.doi.org/10.1021/acs.jpcc.0c02908
J. Phys. Chem. C 2020, 124, 11722−11729

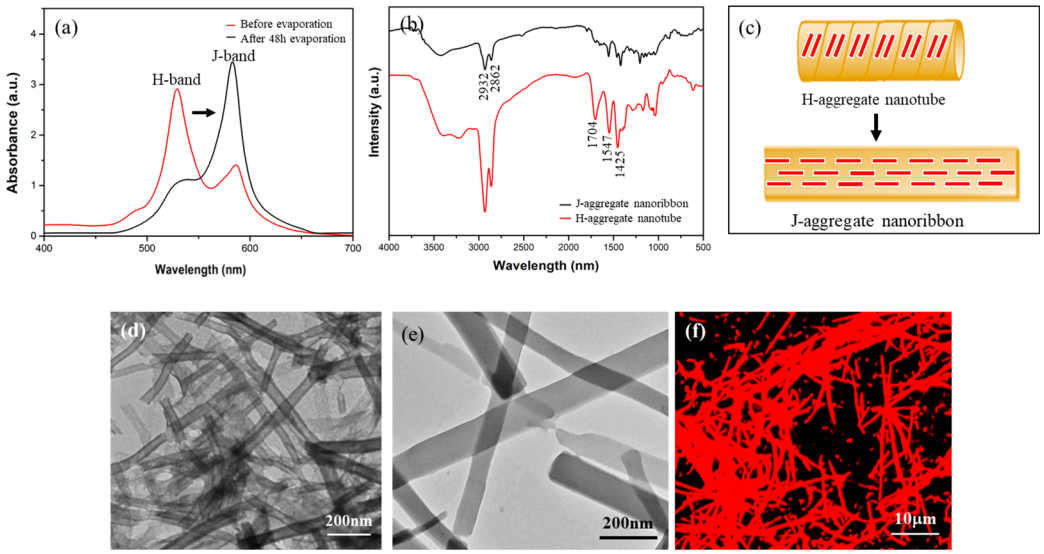

Figure 2. (a) Adsorption spectra of LCA/$DiSC_2(3)$ solution with mixed molar ratio of 5:1 before and after 48 h evaporation of ammonia at room temperature. (b) FT-IR spectra of H-aggregate nanotubes and J-aggregate nanoribbons. (c) Schematic representation of H-aggregate nanotube to J-aggregate nanoribbon transition. TEM images of H-aggregate nanotubes (d) and flat J-aggregate nanoribbons (e). (f) Fluorescent microscopy image of flat J-aggregate nanoribbons.

same time, the H-band at 540 nm significantly increased and slightly shifted to 530 nm during the coassembly process. In this case, a strong H-band at 530 nm and a weak J-band at 585 nm were observed. The time-dependent absorption spectra had an isosbestic point at 510 nm, which represented the equilibrium between two H-aggregates. TEM images revealed the coassembly of LCA and $DiSC_2(3)$ into twisted nanoribbons in the early stage (Figure 1d). Over time, we observed helical nanoribbons, which tended to further twist into nanotubes (Figure 1e). Combining these with the results from the time-dependent absorption spectra, we concluded that the majority of $DiSC_2(3)$ formed H-aggregates in helical nanoribbons and nanotubes.

The physiological function of bile acids is to solubilize dietary lipids in the small intestine by forming mixed micelles through hydrophobic imteraction.[29] The micelles can further aggregate via hydrogen bonding with the increase of bile acid concentrations. It was reported that guest molecules could be incorporated in the cavity of bile acid micelles.[32,33] Thus, we assumed that $DiSC_2(3)$ molecules were incorporated in the cavity of LCA micelles through hydrophobic interaction. The mixed LCA/$DiSC_2(3)$ micelles then assembled into nanoribbons, in which $DiSC_2(5)$ formed H-aggregates. The chiral interaction of LCA twisted H-aggregate nanoribbons into H-aggregate nanotubes (Figure 1f).

There was no change in the H-band at 530 nm if the H-aggregate nanotube solution was sealed in a glass bottle for a weak. Interestingly, 48 h of evaporation of ammonia from H-aggregate solution in an open glass bottle at room temperature caused a significant decrease of the H-band at 530 nm. At the same time, the J-band at 585 nm intensified (Figure 2a), suggesting that the ammonia evaporation triggered the H- to J-aggregate transition. Our controlled experiments confirmed that the H- to J-aggregate transition occurred after 20 h of evaporation of ammonia (Figure S3a). The J-aggregates showed a narrow emission at 592 nm, which was slightly shifted with respect to the J-band (Figure 2b). The H-aggregate nanotubes had an external diameter in the range from 50 to 70 nm and a wall thickness of ~12 nm (Figure 2b). After 48 h of evaporation of ammonia, the H-aggregate nanotubes transitioned into flat J-aggregate nanoribbons with the width from 110 to 180 nm (Figure 2c).

FT-IR spectra of H-aggregate nanotubes and J-aggregate nanoribbons are shown in Figure 2d. The broad peak in the region between 3100 and 3500 cm^{-1} represented the stretching of the OH group of LCA. The peaks at 2862 and 2932 cm^{-1} correspond to the stretching of the CH_2 group in the alkyl chain of $DiSC_{2n}(3)$ and LCA. The peak at 1420 cm^{-1} was attributed to the C═C stretching of the central conjugated chain of $DiSC_2(3)$.[34] The main difference of the FT-IR spectra between H-aggregate nanotubes and J-aggregate nanoribbons was in the carbonyl stretching region. H-aggregate nanotubes showed a peak at 1546 cm^{-1}, which could be assigned to the stretching of the COO− group of LCA. In addition to the peak at 1546 cm^{-1}, flat J-aggregate nanoribbons showed a peak at 1704 cm^{-1}, which was due to the stretching of the COOH group. It was reported that the nonassociated COOH group showed the absorption peak at ~1750 cm^{-1} and the association of COOH groups through hydrogen bonding showed a peak at ~1700 cm^{-1}.[35] On the basis of the FT-IR data, we concluded that the COOH group of some LCA molecules formed via hydrogen bonding in flat J-aggregate nanoribbons. Mesoscale simulations showed that the shape of the nanoribbons of chiral amphiphiles was determined by the balance between their elasticity and chirality.[36] The chiral interaction of LCA was the main driving force for twisting nanoribbons into nanotubes. The cooperation of hydrophobic interaction, hydrogen bonding, and electrostatic interaction of LCA and $DiSC_2(3)$ contributed to the elasticity of H-aggregate nanotubes. Ammonia is a weak base. In ammonia solution, a small amount of ammonia converts to ammonium ions by the deprotonation of water according to the following equilibrium equation: $NH_3 + H_2O \rightleftharpoons NH_4^+ + OH^-$. It is well-known that the ionization constant of the COOH group of LCA depends on its local environment. The pK_a value of LCA in crystalline monolayers is ~8.4.[37] In 30% ammonia solution with pH 13.1, LCA was deprotonated in H-aggregate nanoribbons, which is evident in Figure 2d. The pH

https://dx.doi.org/10.1021/acs.jpcc.0c02908
J. Phys. Chem. C 2020, 124, 11722−11729

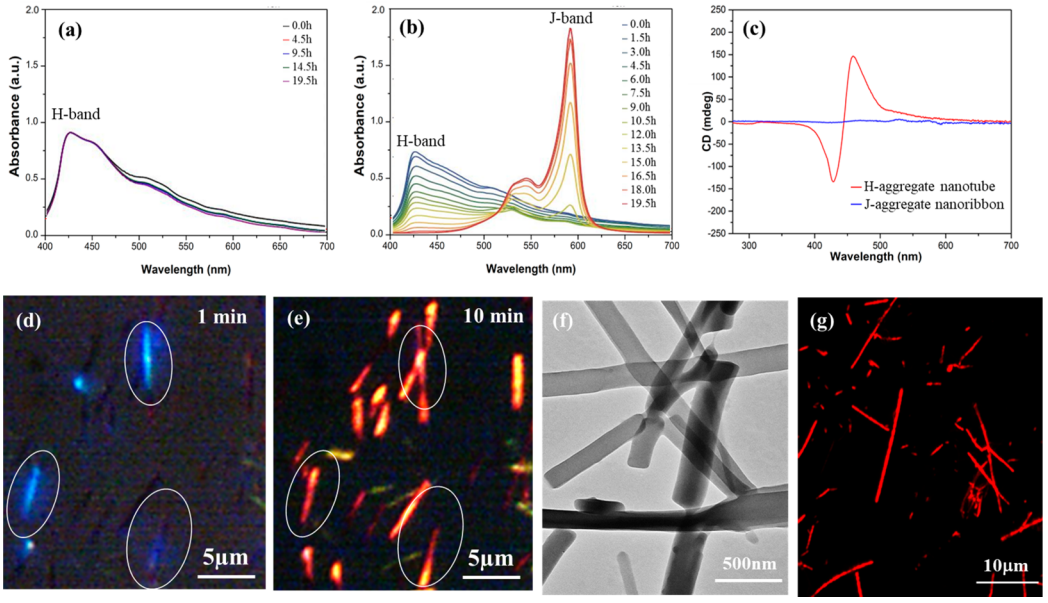

Figure 3. Time-dependent adsorption spectra of LCA/DiSC$_2$(3) solution with a mixed molar ratio of 1:1 in a sealed (a) and an open (b) glass bottle at room temperature. (c) Circular dichroism spectra of H-aggregate nanotubes and J-aggregate nanoribbons. (d, e) In situ polarizing optical microscopy images of H-aggregate nanotubes during the drying of ammonia solution on a glass substrate. (f) TEM image of J-aggregate nanoribbons after being dried on a holey Formvar film. (g) Fluorescent microscopy image of flat J-aggregate nanoribbons after being dried on a glass substrate.

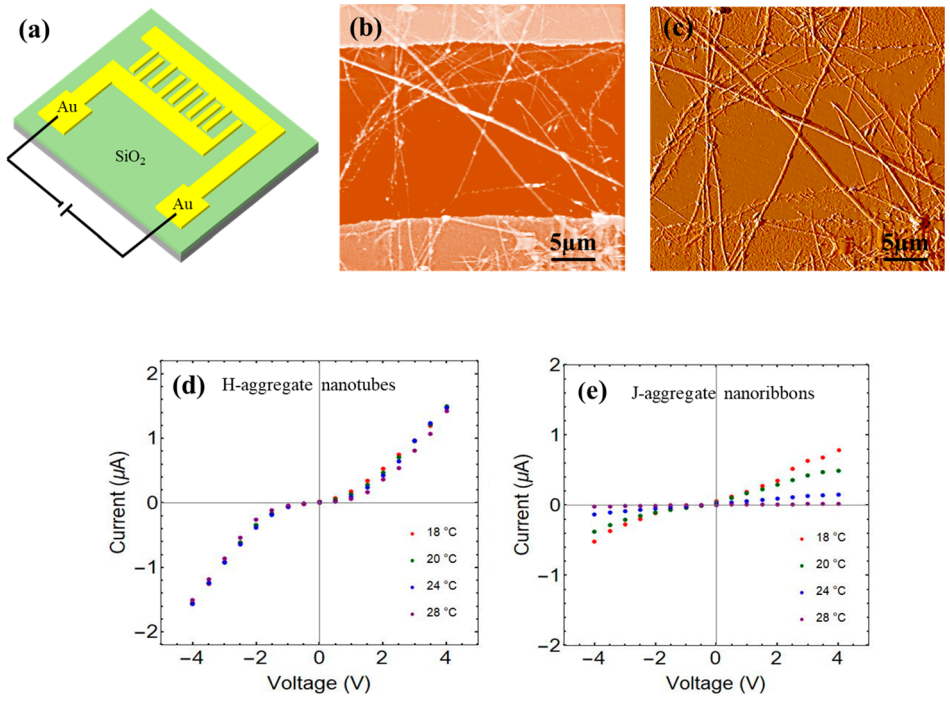

Figure 4. (a) Schematic illustration of the fabrication of interdigitated gold electrodes. Topography (b) and amplitude (c) mode AFM images of H-aggregate nanotubes bridging the 20 μm gap between interdigitated gold electrodes. Temperature-dependent $I-V$ curves of H-aggregate nanotubes (d) and J-aggregate nanoribbons (e).

of the ammonia solution decreased to 9.1 after 48 h of evaporation of ammonia. As can be seen in Figure 2b, some LCA molecules were protonated. The hydrogen bonding of protonated LCA molecules in the H-aggregate nanotubes disrupted the balance between the chiral interaction and the elasticity; the chiral interaction of LCA molecules was unable to overcome the elastic energy, leading to the nanotube-to-nanoribbon transition. The transition from nanotubes to flat nanoribbons caused the H- to J-aggregate transition of DiSC$_2$(3) to integrate in them (Figure 2e). As we expected, the J-aggregate nanoribbons were highly fluorescent (Figure 2f).

When the mixed molar ratio of LCA and DiSC$_2$(3) in 30% ammonia solution was changed to 1:1, for which the concentration of LCA was still maintained at 1 mM, a broad absorbance with a maximum at 425 nm was observed 24 h

https://dx.doi.org/10.1021/acs.jpcc.0c02908
J. Phys. Chem. C 2020, 124, 11722−11729

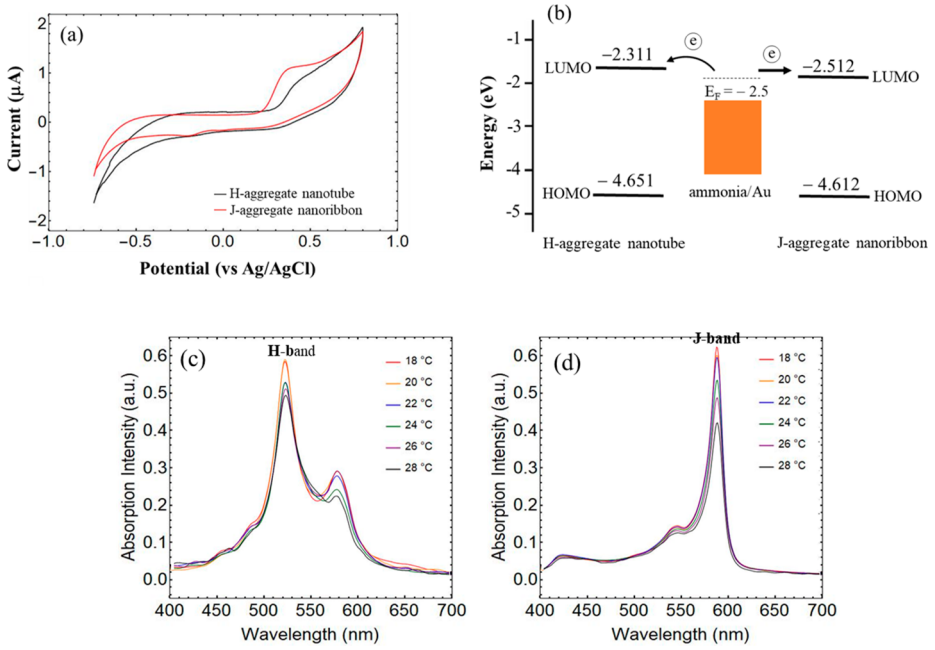

Figure 5. (a) Cyclic voltammograms of H-aggregate nanotubes and J-aggregate nanoribbons. (b) Energy levels of H-aggregate nanotubes and J-aggregate nanoribbons, together with the Fermi energy of ammonia-coated Au substrates for comparison. Temperature-dependent adsorption spectra of H-aggregate nanotubes (c) and J-aggregate nanoribbons (d) in solution.

after the mixed LCA/$DiSC_2(3)$ solution was made (Figure 3a). The maximum absorbance at 425 nm was blue-shifted with respect to the monomer band, suggesting the formation of H-aggregates of $DiSC_2(3)$. There was no change in the adsorption spectrum if the H-aggregate solution was sealed in a glass bottle over time (Figure 3a). However, the evaporation of ammonia from an open glass bottle at room temperature triggered the H- to J-aggregate transition (Figure 3b). The H- to J-aggregate transition completed after 18 h of evaporation of ammonia, during which the H-band disappears. The kinetics of the H- to J-aggregate transition at the mixed molar ratio of 1:1 is faster than that at 5:1. The H-aggregate nanotubes showed a split circular dichroism (CD) signal with a positive Cotton effect at 460 nm and a negative Cotton effect at 430 nm (Figure 3c). The split CD signal suggests the chiral excitonic coupling of achiral $DiSC_2(3)$ in the H-aggregate nanotubes. The H-aggregate nanotubes were formed through helical H-aggregate nanoribbons. Thus, we concluded that the chiral excitonic coupling of $DiSC_2(3)$ reflected a helical arrangement of $DiSC_2(3)$ in the H-aggregate nanotubes, but flat J-aggregates gave no CD signal (Figure 3c).

Because of the fast transition kinetics at a mixed molar ratio of 1:1, the H- to J-aggregate transition could be in situ monitored with a POM during the drying of a drop of H-aggregate solution onto a glass substrate at room temperature. As can be seen in the POM image shown in Figure 3d, three H-aggregate nanotubes marked with white circles initially showed blue color and then turned into yellow color (Figure 3e). The different colors of H- and J-aggregates in POM images could be explained by their different absorption regions.[38] Thus, white light illumination under POM can provide different transmissions of colors. After the H-aggregate solution was dried on substrates, flat J-aggregate nanoribbons were observed (Figure 3f). Occasionally, partially open H-aggregate nanotubes were observed as well, suggesting the transition from H-aggregate nanotubes to J-aggregate nanoribbons occurred during the drying process, during which the ammonia quickly evaporated. The J-aggregate nanotubes showed strong fluorescence (Figure 3g). However, because of the slow transition kinetics at the mixed molar ratio of 5:1, the H-aggregate nanotubes remained intact even after being dried on substrates (Figure 2d). The H- to J-aggregate transition was reversible when the J-aggregate nanoribbons were resuspended in 30% ammonia solution (Figure S4). The H- to J-aggregate transition was also observed in other aggregation systems.[39−41]

The length of the H-aggregate nanotubes formed at the mixed LCA/$DiSC_2(3)$ molar ratio of 1:1 was shorter than the gap (20 μm) of the interdigitated gold electrodes fabricated on a SiO_2 substrate (Figure S5). Thus, we measured the electrical properties of the H-aggregate nanotubes and the J-aggregate nanoribbons formed at a mixed LCA/$DiSC_2(3)$ molar ratio of 5:1 by deposition onto the interdigitated gold electrodes (Figure 4a). The bridging of the deposited H-aggregate nanotubes to the gap between the gold electrodes was confirmed by atomic force microscope (AFM). As can be seen from the height mode AFM image shown in Figure 4b, the H-aggregate nanotubes appeared to be flexible and bent at the edges of the protruded gold electrodes to conform to the topography of the electrodes. The amplitude mode AFM image, which was taken simultaneously with the height mode AFM image during the scanning, revealed that there was no break for the bent H-aggregate nanotubes (Figure 4c). The $I-V$ curves of the H-aggregate nanotubes were nonlinear with a threshold voltage of ~1.2 V (Figure 4d). Above the threshold, the current showed a near linear increase with an increase of voltage. The nonlinear $I-V$ curve suggested a Schottky contact between the H-aggregate nanotubes and the gold electrodes. In contrast, the $I-V$ curves of J-aggregate nanoribbons were linear (Figure 4e), suggesting Ohmic contact with the gold electrode. The $I-V$ curves of the H-aggregate nanotubes essentially overlapped with the increase of temperature from 18 to 28 °C

https://dx.doi.org/10.1021/acs.jpcc.0c02908
J. Phys. Chem. C 2020, 124, 11722−11729

(Figure 4d). However, the $I-V$ curves of J-aggregate nanoribbons were dependent on the temperature (Figure 4e). The resistance of the H-aggregate nanotubes was calculated from the slope of the linear part of the $I-V$ curves. With the increase of temperature from 18 to 28 °C, the resistance of the H-aggregate nanotubes was nearly constant at ∼4 MΩ, whereas the J-aggregate nanoribbons showed a significant increase in their resistance from ∼6 to ∼190 MΩ.

The different contacts of gold electrodes with the J-aggregate nanotubes and the H-aggregate nanoribbons could be explained on the basis of their different energy levels with respect to the Fermi energy of gold electrodes. The cyclic voltammetry (CV) curves of the H-aggregate nanotubes and the J-aggregate nanoribbons adsorbed on indium tin oxide coated glass substrates in aqueous solution containing 1 M KNO_3 were measured. The oxidized potentials of the H-aggregate nanotubes and the J-aggregate nanoribbons were ∼0.31 and ∼0.22 V, respectively (Figure 5a). The highest occupied molecular orbital (HOMO) and the lowest unoccupied molecular orbital (LUMO) levels of the H-aggregate nanotubes and the J-aggregate nanoribbons were estimated from the following empirical equations:[42]

$$E(\mathrm{HOMO}) = -e(E_{\mathrm{onset}} + 4.4) \quad (1)$$

$$E(\mathrm{LUMO}) = E_{\mathrm{g}} - E(\mathrm{HOMO}) \quad (2)$$

where the E_{onset} is the oxidation potential, which was 0.31 V for the H-aggregate nanotubes and 0.22 V for the J-aggregate nanoribbons, respectively. E_{g} is the optical band gap energy that could be calculated according to the equation $E_{\mathrm{g}} = 1242/\lambda_{\mathrm{onset}}$. For the H-aggregate nanotubes with the sharp H-band at 530 nm, E_{g} was calculated to be ∼2.34 eV. For the J-aggregate nanoribbons with the sharp J-band at 585 nm, E_{g} was calculated to be ∼2.10 eV. With use of the empirical equations, the E(HOMO) and E(LUMO) levels of the H-aggregate nanotubes were estimated to be −4.65 and −2.31 eV, respectively. The E(HOMO) and E(LUMO) levels of the J-aggregate nanoribbons were estimated to be −4.61 and −2.51 eV, respectively. The Fermi energy of gold is −4.4 eV in an ambient atmosphere.[43] It was reported that a quarter monolayer coverage of ammonia could reduce the work function of gold by 1.9 eV.[44] In 30% ammonia solution, the adsorption of ammonia on the Au electrodes is expected. By assuming a quarter monolayer coverage of ammonia, we could infer that the Fermi energy of the ammonia-coated Au electrodes was −2.5 eV. A schematic energy level diagram of the H-aggregate nanotubes and the J-aggregate nanoribbons together with the Fermi energy of ammonia-coated gold electrodes is shown in Figure 5b. The Fermi energy of the ammonia-coated gold electrode was lower than the LUMO level (− 2.311 eV) of the H-aggregate nanotubes, favoring Schottky contact. A large voltage was required to remove the difference and make the electronic injection from the Au electrode to the H-aggregate nanotubes. However, the Fermi energy level of ammonia-coated gold electrodes was very close to the LUMO level (− 2.512 eV) of the J-aggregate nanoribbons, favoring Ohmic contact. The electrons could be free to flow across the contact from the gold electrode to the J-aggregate nanoribbons with negligible contact resistance.

To understand the effect of temperature on the resistance of the H-aggregate nanotubes and the J-aggregate nanoribbons, we measured the temperature-dependent absorption spectra of the H-aggregate nanotubes and the J-aggregate nanoribbons in solution. Upon heating of the solution from 18 to 28 °C at a rate of 5 °C/min, the intensity of the H-band decreased ∼12% (Figure 5c), whereas the intensity of the J-band dropped ∼37% (Figure 5d) without the appearance of new bands. This behavior was reversible. Thus, we concluded that the large decrease of the J-band intensity was a result of the weakening of the J-coupling of $DiSC_2(3)$ in the nanoribbons, which might explain the increase of the resistance of the J-aggregate nanoribbons with the increase of temperature. The data shown in Figure 5c,d also suggested that the H-coupling of $DiSC_2(3)$ in the nanotubes was stronger than the J-coupling of $DiSC_2(3)$ in the nanoribbons, which agreed with the results from the stability studies showing the J- and H-aggregates formed within the groove of DNA templets.[45] The temperature-dependent $I-V$ curves of the J-aggregate nanoribbons were reversible over multiple cycles in the range from 18 to 28 °C. However, when the temperature was increased to 32 °C, there was no current observed through both the H-aggregate nanotubes and the J-aggregate nanoribbons because of the breaking of the coupling of $DiSC_2(3)$ molecules.

CONCLUSIONS

We have shown that the coassembly of LCA and $DiSC_2(3)$ in 30% ammonia solution can form H-aggregate nanotubes through helical H-aggregate nanoribbons. The H-aggregate nanotubes transition into flat J-aggregate nanoribbons as the ammonia evaporates. The H- to J-aggregate transition is a result of the formation of the hydrogen bonding of LCA, which strengthens the nanoribbons; the chiral interaction of LCA is unable to twist the nanoribbons into nanotubes. The kinetics of the H- to J-aggregate transition depends on the LCA/$DiSC_2(3)$ mixed molar ratios. After being integrated with interdigitated gold electrodes, the H-aggregate nanotubes form a Schottky junction, whereas the J-aggregate nanoribbons form an Ohmic junction. In the temperature range from 18 to 28 °C. The resistance of the H-aggregate nanotubes remains nearly constant, whereas the resistance of the J-aggregate nanoribbons increases with the increase in temperature due to the weakening of the J-coupling of $DiSC_2(3)$ in the nanoribbons. Our findings reveal a simple way for controlling the formation of H-aggregate nanotubes and J-aggregate nanoribbons, which show great potential as functional nanomaterials in electronic and optoelectronic devices.

ASSOCIATED CONTENT

Supporting Information

The Supporting Information is available free of charge at https://pubs.acs.org/doi/10.1021/acs.jpcc.0c02908.

Materials, methods for the fabrication of interdigitated gold electrodes, and adsorption spectra (PDF)

AUTHOR INFORMATION

Corresponding Author

Jiyu Fang − *Advanced Materials Processing and Analysis Center and Department of Materials Science and Engineering, University of Central Florida, Orlando, Florida 32816, United States;* orcid.org/0000-0002-6056-5113; Email: Jiyu.Fang@ucf.edu

Authors

Samuel Rhodes − *Advanced Materials Processing and Analysis Center and Department of Materials Science and Engineering,*

https://dx.doi.org/10.1021/acs.jpcc.0c02908
J. Phys. Chem. C 2020, 124, 11722−11729

University of Central Florida, Orlando, Florida 32816, United States

Wenlang Liang − *College of Materials Science and Engineering, Southwest Jiaotong University, Chengdu, Sichuan 610031, P.R. China*

Xiaochen Wang − *Advanced Materials Processing and Analysis Center and Department of Materials Science and Engineering, University of Central Florida, Orlando, Florida 32816, United States*

Nitin Ramesh Reddy − *Advanced Materials Processing and Analysis Center and Department of Materials Science and Engineering, University of Central Florida, Orlando, Florida 32816, United States*

Complete contact information is available at: https://pubs.acs.org/10.1021/acs.jpcc.0c02908

Author Contributions

#S.R. and W.L. contributed equally to this work.

Notes

The authors declare no competing financial interest.

■ ACKNOWLEDGMENTS

This work was supported by the U.S. National Science Foundation (CBET 1803690).

■ REFERENCES

(1) Hoeben, F. J. M.; Jonkheijm, P.; Meijer, E. W.; Schenning, A. About Supramolecular Assemblies of π-Conjugated Systems. *Chem. Rev.* **2005**, *105*, 1491−1546.

(2) Faramarzi, V.; Niess, F.; Moulin, E.; Maaloum, M.; Dayen, J. F.; Beaufrand, J. B.; Zanettini, S.; Doudin, B.; Giuseppone, N. Light-Triggered Self-Construction of Supramolecular Organic Nanowires as Metallic Interconnects. *Nat. Chem.* **2012**, *4*, 485−490.

(3) Haedler, A. T.; Kreger, K.; Issac, A.; Wittmann, B.; Kivala, M.; Hammer, N.; Köhler, J.; Schmidt, H. W.; Hildner, R. Long-Range Energy Transport in Single Supramolecular Nanofibres at Room Temperature. *Nature* **2015**, *523*, 196−199.

(4) Jain, A.; George, S. J. New Directions in Supramolecular Electronics. *Mater. Today* **2015**, *18*, 206−214.

(5) Li, X.; Wolanin, P. J.; MacFarlane, L. R.; Harniman, R. L.; Qian, J.; Gould, O. E. C.; Dane, T. G.; Rudin, J.; Cryan, M. J.; Schmaltz, T.; Frauenrath, H.; Winnik, M. A.; Faul, C. F. J.; Manners, I. Uniform Electroactive Fibre-Like Micelle Nanowires for Organic Electronics. *Nat. Commun.* **2017**, *8*, 15909.

(6) Würthner, F.; Kaiser, T. E.; Saha-Möller, C. R. J-Aggregates: From Serendipitous Discovery to Supramolecular Engineering of Functional Dye Materials. *Angew. Chem., Int. Ed.* **2011**, *50*, 3376−3410.

(7) von Berlepsch, H.; Böttcher, C.; Ouart, A.; Burger, C.; Dähne, S.; Kirstein, S. Supramolecular Structures of J-Aggregates of Carbocyanine Dyes in Solution. *J. Phys. Chem. B* **2000**, *104*, 5255−5262.

(8) Lang, E.; Sorokin, A.; Drechsler, M.; Malyukin, Y. V.; Köhler, J. Optical Spectroscopy on Individual Amphi-PIC J-Aggregates. *Nano Lett.* **2005**, *5*, 2635−2640.

(9) Eisele, D. M.; Cone, W.; Bloemsma, E. A.; Vlaming, S. M.; vanderKwaak, C. G. F.; Silbey, R. J.; Bawendi, M. G.; Knoester, J.; Rabe, J. P.; Vanden Bout, D. A. Utilizing Redox-Chemistry to Elucidate the Nature of Exciton Transitions in Supramolecular Dye Nanotubes. *Nat. Chem.* **2012**, *4*, 655−662.

(10) Yuen-Zhou, J.; Arias, D. H.; Eisele, D. M.; Steiner, C. P.; Krich, J. J.; Bawendi, M. G.; Nelson, K. A.; Aspuru-Guzik, A. Coherent Exciton Dynamics in Supramolecular Light-Harvesting Nanotubes Revealed by Ultrafast Quantum Process Tomography. *ACS Nano* **2014**, *8*, 5527−5534.

(11) Clark, K. A.; Krueger, E. L.; Vanden Bout, D. A. Direct Measurement of Energy Migration in Supramolecular Carbocyanine Dye Nanotubes. *J. Phys. Chem. Lett.* **2014**, *5*, 2274−2282.

(12) Eisele, D. M.; Arias, D. H.; Fu, X.; Bloemsma, E. A.; Steiner, C. P.; Jensen, R. A.; Rebentrost, P.; Eisele, H.; Tokmakoff, A.; Lloyd, S.; Nelson, K. A.; Nicastro, D.; Knoester, J.; Bawendi, M. G. Robust Excitons Inhabit Soft Supramolecular Nanotubes. *Proc. Natl. Acad. Sci. U. S. A.* **2014**, *111*, E3367−E3375.

(13) Kriete, B.; Bondarenko, A. S.; Jumde, V. R.; Franken, L. E.; Minnaard, A. J.; Jansen, T. L. C.; Knoester, J.; Pshenichnikov, M. S. Steering Self-Assembly of Amphiphilic Molecular Nanostructures via Halogen Exchange. *J. Phys. Chem. Lett.* **2017**, *8*, 2895−2901.

(14) Chen, Z.; Liu, Y.; Wagner, W.; Stepanenko, V.; Ren, X.; Ogi, S.; Würthner, F. Near-IR Absorbing J-Aggregate of an Amphiphilic BF2 Azadipyrromethene Dye by Kinetic Cooperative Self-Assembly. *Angew. Chem., Int. Ed.* **2017**, *56*, 5729−5733.

(15) Kriete, B.; Lüttig, J.; Kunsel, T.; Malý, P.; Jansen, T. L. C.; Knoester, J.; Brixner, T.; Pshenichnikov, M. S. Interplay Between Structural Hierarchy and Exciton Diffusion in Artificial Light Harvesting. *Nat. Commun.* **2019**, *10*, 4615.

(16) von Berlepsch, H.; Böttcher, C.; Ouart, A.; Regenbrecht, M.; Akari, S.; Keiderling, U.; Schnablegger, H.; Dähne, S.; Kirstein, S. Surfactant-Induced Changes of Morphology of J-Aggregates: Super-helix-to-Tubule Transformation. *Langmuir* **2000**, *16*, 5908−5916.

(17) Wang, Z.; Medforth, C. J.; Shelnutt, J. A. Porphyrin Nanotubes by Ionic Self-Assembly. *J. Am. Chem. Soc.* **2004**, *126*, 15954−15955.

(18) Ryu, N.; Okazaki, Y.; Pouget, E.; Takafuji, M.; Nagaoka, S.; Ihara, H.; Oda, R. Fluorescence Emission Originated from the H-Aggregated Cyanine Dye with Chiral Gemini Surfactant Assemblies Having a Narrow Absorption Band and a Remarkably Large Stokes Shift. *Chem. Commun.* **2017**, *53*, 8870−8875.

(19) Guralchuk, G. Y.; Katrunov, I. K.; Grynyov, R. S.; Sorokin, A. V.; Yefimova, S. L.; Borovoy, I. A.; Malyukin, Y. V. Anomalous Surfactant-Induced Enhancement of Luminescence Quantum Yield of Cyanine Dye J-Aggregates. *J. Phys. Chem. C* **2008**, *112*, 14762−14768.

(20) Kameta, N.; Ishikawa, K.; Masuda, M.; Asakawa, M.; Shimizu, T. Soft Nanotubes Acting as a Light-Harvesting Antenna System. *Chem. Mater.* **2012**, *24*, 209−214.

(21) Liang, W.; He, S.; Fang, J. Y. Self-Assembly of J-Aggregate Nanotubes and Their Applications for Sensing Dopamine. *Langmuir* **2014**, *30*, 805−811.

(22) Terech, P.; Jean, B.; Ne, F. Hexagonally Ordered Ammonium Lithocholate Self-Assembled Nanotubes with Highly Monodisperse Solution. *Adv. Mater.* **2006**, *18*, 1571−1574.

(23) Pal, A.; Basit, H.; Sen, S.; Aswal, V. K.; Bhattacharya, S. J. Structure and Properties of Two Component Hydrogels Comprising Lithocholic Acid and Organic Amines. *J. Mater. Chem.* **2009**, *19*, 4325−4334.

(24) Zhang, X.; Zou, J.; Tamhane, K.; Kobzeff, F.; Fang, J. Y. Self-Assembly of pH-Switchable Spiral Tubes: Supramolecular Chemical Springs. *Small* **2010**, *6*, 217−220.

(25) Tamhane, K.; Zhang, X.; Zou, J.; Fang, J. Assembly and Disassembly of Tubular Spherulites. *Soft Matter* **2010**, *6*, 1224−1228.

(26) Terech, P.; Velu, S. K. P.; Pernot, P.; Wiegart, L. Salt Effects in the Formation of Self-Assembled Lithocholate Helical Ribbons and Tubes. *J. Phys. Chem. B* **2012**, *116*, 11344−11355.

(27) Wang, H.; Xu, W.; Song, S.; Feng, L.; Song, A.; Hao, J. Hydrogels Facilitated by Monovalent Cations and Their Use as Efficient Dye Adsorbents. *J. Phys. Chem. B* **2014**, *118*, 4693−4701.

(28) di Gregorio, M. C.; Travaglini, L.; Del Giudice, A.; Cautela, J.; Pavel, N. V.; Galantini, L. Bile Salts: Natural Surfactants and Precursors of a Broad Family of Complex Amphiphiles. *Langmuir* **2019**, *35* (21), 6803−6821.

(29) Hofmann, A. F.; Rods, A. Physicochemical Properties of Bile Acids and Their Relationship to Biological Properties: An Overview of the Problem. *J. Lipid Res.* **1984**, *25*, 1477−1489.

(30) Iwata, K.; Weaver, W. L.; Gustafson, T. L. Spontaneous Raman Spectra of the Cyanine Dye DODCI and Its Six Analogues Using

Titanium: Sapphire Laser Excitation. *J. Phys. Chem.* **1992**, *96*, 10219−10224.
(31) Rhodes, S.; Liang, W.; Shteinberg, E.; Fang, J. Y. Formation of Spherulitic J-Aggregates from the Coassembly of Lithocholic Acid and Cyanine Dye. *J. Phys. Chem. Lett.* **2017**, *8*, 4504−4509.
(32) Li, G.; McGown, L. B. A New Approach to Polydispersity Studies of Sodium Taurocholate and Sodium Taurodeoxycholate Aggregates using Dynamic Fluorescence Anisotropy. *J. Phys. Chem.* **1993**, *97*, 6745−6752.
(33) Ju, C.; Bohne, C. Dynamics of Probe Complexation to Bile Salt Aggregates. *J. Phys. Chem.* **1996**, *100*, 3847−3854.
(34) Iwata, K.; Weaver, W. L.; Gustafson, T. L. Spontaneous Raman Spectra of the Cyanine Dye. *J. Phys. Chem.* **1992**, *96*, 10219−10224.
(35) Lichkus, M.; Painter, P. C.; Coleman, M. M. Hydrogen Bonding in Polymer Blends. 5. Blends Involving Polymers Containing Methacrylic Acid and Oxazoline Groups. *Macromolecules* **1988**, *21*, 2636−2641.
(36) Selinger, R. L. B.; Selinger, J. V.; Malanoski, A. P.; Schnur, J. M. Shape Selection in Chiral Self-Assembly. *Phys. Rev. Lett.* **2004**, *93*, 158103.
(37) Leonard, M. R.; Bogle, M. A.; Carey, M. C.; Donovan, J. M. Spread Monomolecular Films of Monohydroxy Bile Acids and Their Salts: Influence of Hydroxyl Position, Bulk pH, and Association with Phosphatidylcholine. *Biochemistry* **2000**, *39*, 16064−16074.
(38) Yao, H.; Domoto, K.; Isohashi, T.; Kimura, K. In situ Detection of Birefringent Mesoscopic H and J Aggregates of Thiacarbocyanine Dye in Solution. *Langmuir* **2005**, *21*, 1067−1073.
(39) Yagai, S.; Seki, T.; Karatsu, T.; Kitamura, A.; Würthner, F. Transformation from H- to J-Aggregated Perylene Bisimide Dyes by Complexation with Cyanurates. *Angew. Chem., Int. Ed.* **2008**, *47*, 3367−3371.
(40) Sarbu, A.; Biniek, L.; Guenet, J.-M.; Mésini, P. J.; Brinkmann, M. Reversible J- to H-Aggregate Transformation in Thin Films of a Perylenebisimide Organogelator. *J. Mater. Chem. C* **2015**, *3*, 1235−1242.
(41) Hestand, N. J.; Spano, F. C. Interference between Coulombic and CT-Mediated Couplings in Molecular Aggregates: H- to J-Aggregate Transformation in Perylene-based π-Stacks. *J. Chem. Phys.* **2015**, *143*, 244707.
(42) Bredas, J. L.; Silbey, R.; Boudreaux, D. S.; Chance, R. R. Chain-Length Dependence of Electronic and Electrochemical Properties of Conjugated Systems: Polyacetylene, Polyphenylene, Polythiophene, and Polypyrrole. *J. Am. Chem. Soc.* **1983**, *105*, 6555−6559.
(43) Kahn, A. Fermi Level, Work Function and Vacuum Level. *Mater. Horiz.* **2016**, *3*, 7−10.
(44) Bilić, A.; Reimers, J. R.; Hush, N. S.; Hafner, J. Adsorption of Ammonia on the Gold (111) Surface. *J. Chem. Phys.* **2002**, *116*, 8981−8987.
(45) Chowdhury, A.; Wachsmann-Hogiu, S.; Bangal, P. R.; Raheem, I.; Peteanu, L. A. Characterization of Chiral H- and J-Aggregates of Cyanine Dyes Formed by DNA Templating Using Stark and Fluorescence Spectroscopies. *J. Phys. Chem. B* **2001**, *105*, 12196−12201.

https://dx.doi.org/10.1021/acs.jpcc.0c02908
J. Phys. Chem. C 2020, 124, 11722−11729